Supporting Information for

Cloud-surface coupling alters the morning transition from stable to unstable boundary layer

Tianning Su[1], Zhanqing Li[1], Youtong Zheng[2]

[1]Department of Atmospheric and Oceanic Sciences & ESSIC, University of Maryland, College Park, Maryland 20740, USA

[2]Program in Atmospheric and Oceanic Sciences, Princeton University, Princeton, New Jersey, the United States.

Submission to ***Geophysical Research Letters***

Correspondence to: zli@atmos.umd.edu; tianning@umd.edu

1. Descriptions of datasets:

(1) The profiles of potential temperature

We will use radiosonde measurements to characterize the thermodynamic settings of the PBL. Radiosondes are routinely launched multiple times at the ARM sites. Holdridge et al. (2011) provided technical details about the ARM radiosonde. Using the well-established method developed by Liu and Liang (2010), we retrieved PBLHs over the SGP site based on the vertical profiles of potential temperature from radiosonde measurements. The temperature and moisture profiles are used in a radiative transfer model to generate vertical profiles of heating rate yielding the CTRC rate (Zheng et al., 2018).

(2) Active Remote Sensing of Clouds (ARSCL)

We will use the well-established ARM cloud product, named ARSCL, generated for each ARM site (Clothiaux et al., 2000; Flynn et al., 2017). ARSCL provides the vertical boundaries of clouds by combining data from the MPL, ceilometer, and cloud radar, conveying useful information pertaining to the vertical structure and temporal evolution of clouds (Kollias et al., 2007). For the lowest cloud base, we will use the best estimation from laser-based techniques (i.e., MPL and ceilometer). Due to the attenuation of lidar signals within clouds, the cloud top is typically identified by cloud radar.

(3) Cloud Optical Properties from the Multifilter Shadowband Radiometer (MFRSRCLDOD)

The MFRSRCLDOD product contains cloud optical properties, including cloud optical depth, liquid water path, and effective radius. In particular, cloud optical depth is derived from narrowband irradiance measurements of the multifilter rotating shadowband radiometer. If the liquid water path is available from the microwave radiometer, we can also calculate the effective radius. Otherwise, we assume a default effective radius of 8.0 um.

(4) Radiation budget and surface fluxes

Surface fluxes are critical for PBL development and closely interact with low clouds as the driving force. The Data Quality Assessment for ARM Radiation Data (QCRAD) provides broadband surface irradiance measurements (Long and Shi, 2008). QCRAD provides accurate measurements of downwelling shortwave (SW) and longwave (LW) irradiances following various quality controls. Surface sensible and latent heat fluxes are from the Bulk Aerodynamic Energy Balance Bowen Ratio data product (BAEBBR; Wesely et al., 1995). The BAEBBR product contains the bulk aerodynamic latent and sensible heat fluxes from the Energy Balance Bowen Ratio, which has been evaluated against the eddy correlation flux measurement system (ECOR) measurements (Tang et al., 2019).

(5) Soil moisture

We will use the long-term soil moisture product at the SGP site. The Soil Water and Temperature System (SWATS) has provided soil moisture measurements since 1996. After 2015, the SWATS was replaced with the Soil Temperature and Moisture Profiles (STAMP) system. The soil moisture would greatly affect the surface latent heat fluxes and sensible heat fluxes.

(6) Sixty-meter meteorological tower

There is a 60-m meteorological tower at the SGP site. The towers are used for meteorological, radiological, and other measurements. In-situ measurements of temperature/relative humidity/vapor pressure are made at 2m, 30m, and 60m. These meteorological measurements monitor the evolution of boundary layer thermodynamics.

2. Figures

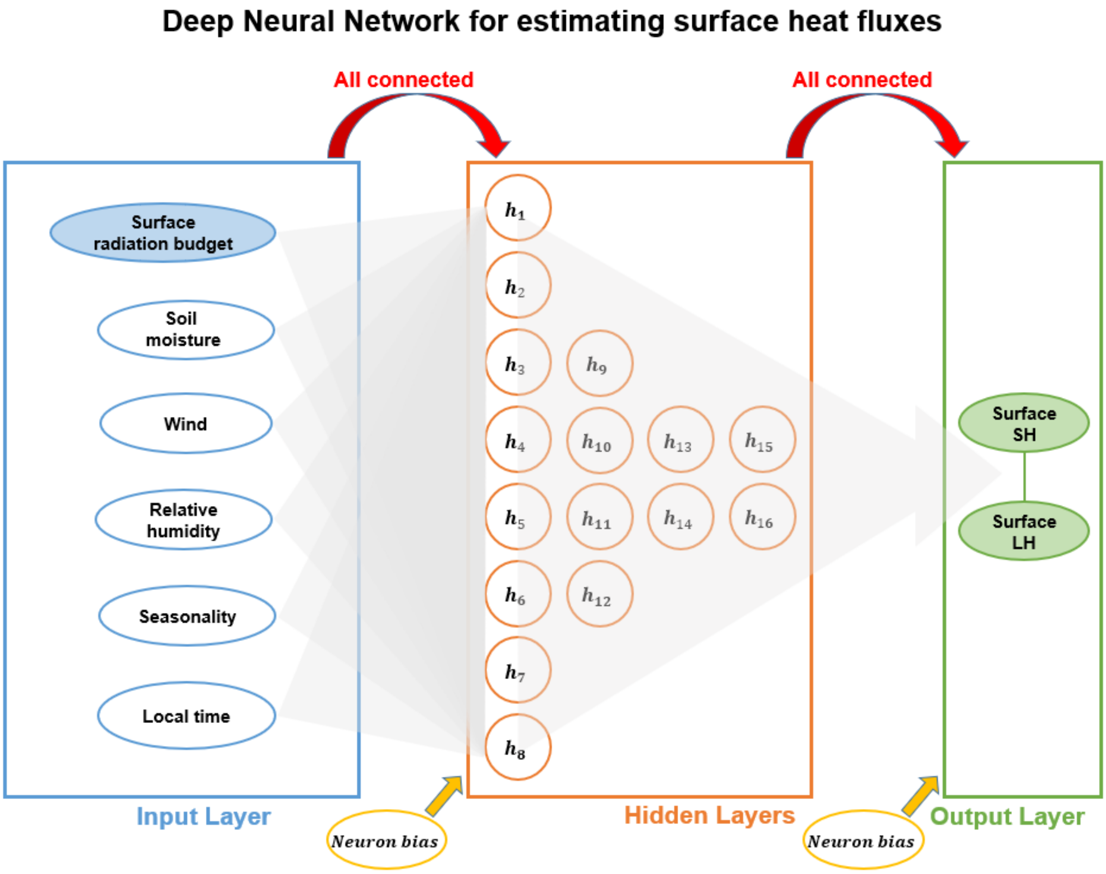

Figure S1. The deep neural network (DNN) diagram to estimate surface heat fluxes (surface sensible heat and surface latent heat). The input data for DNN include net surface radiation budget (QCRAD), 5-cm soil moisture below the surface (volumetric water content), surface wind speed (u and v components), relative humidity, seasonality (month), and local time. The output data in the DNN are sensible and latent heat fluxes at surface. Cloud radiative forcing can affect the surface radiation budget and thus change the surface fluxes.

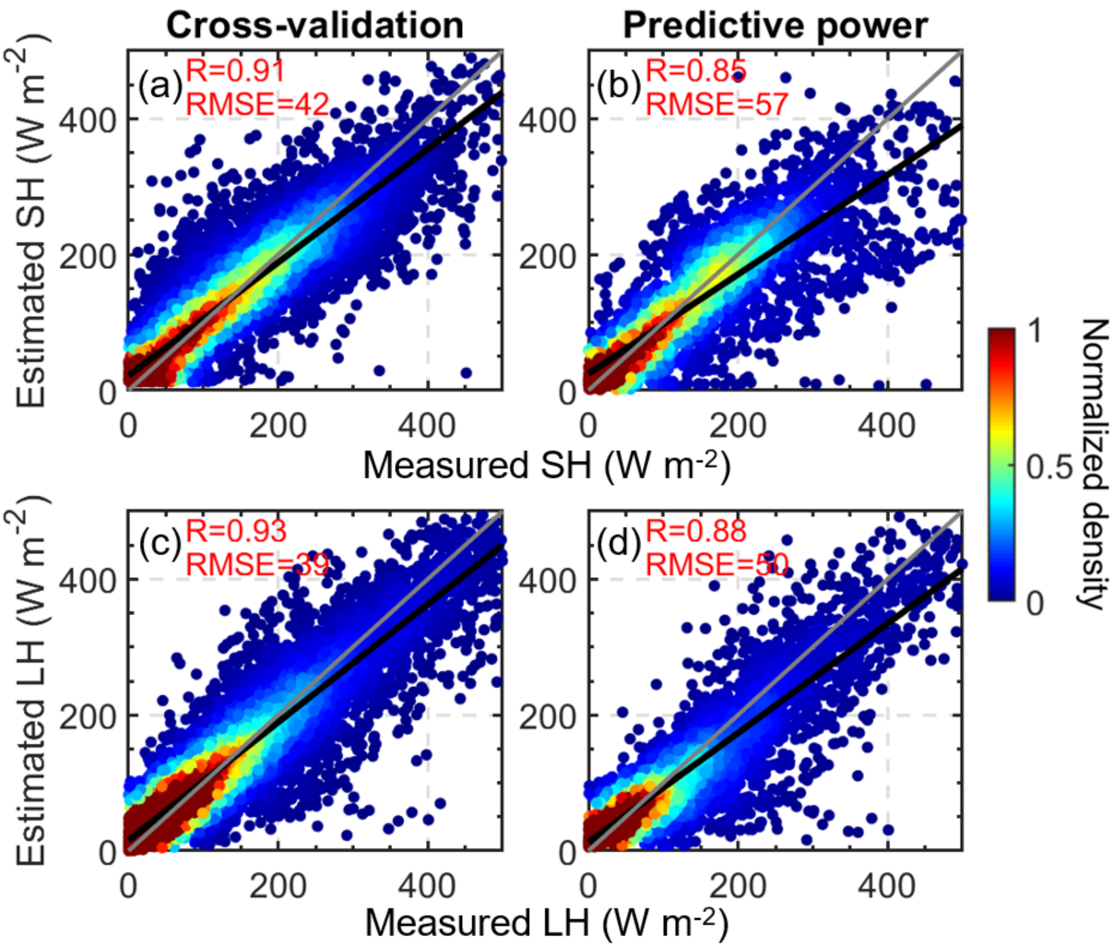

Figure S2. Density scatterplots of the comparison between estimated sensible heat (SH) and measured SH for (a) the 10-fold cross-validation (Rodriguez et al., 2009) and for (b) the predictive power. (c-d) Same as (a-b), but for the latent heat (LH). The correlation coefficients (R) and Root Mean Square Error (RMSE) are given in each panel. The solid black lines represent the linear regression, and the dashed grey lines denote 1:1 line. For testing the model's predictive power, we use the model built for 1999-2011 to forecast surface fluxes during 2012-2018 and validate the forecast data with ground truth.

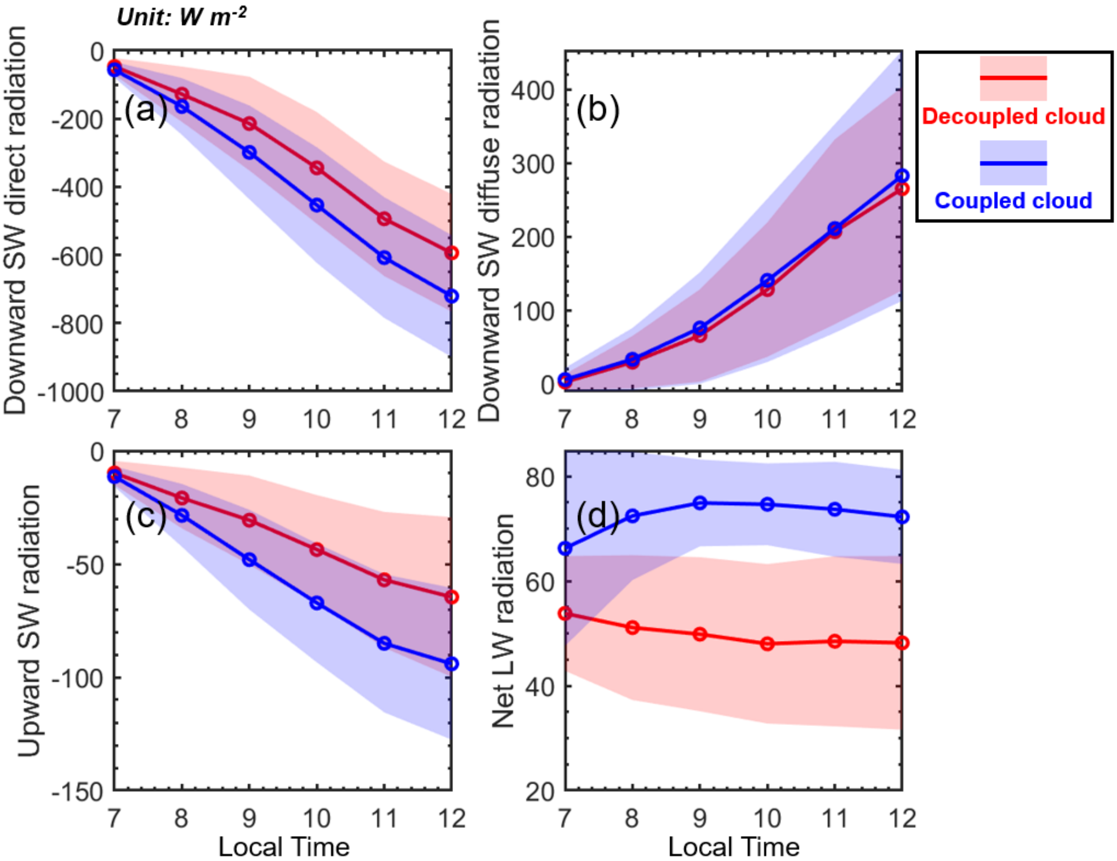

Figure S3. (a) Variations of the cloud radiative forcing (CRF) for downward SW radiation (direct beam only) at the surface level under coupling and decoupling conditions during 07:00-12:00 LT. (b) Same as (a), but for the downward SW diffuse radiation at surface. (c) Same as (a), but for the upward SW radiation at surface. (d) Same as (a), but for net LW radiation at surface.

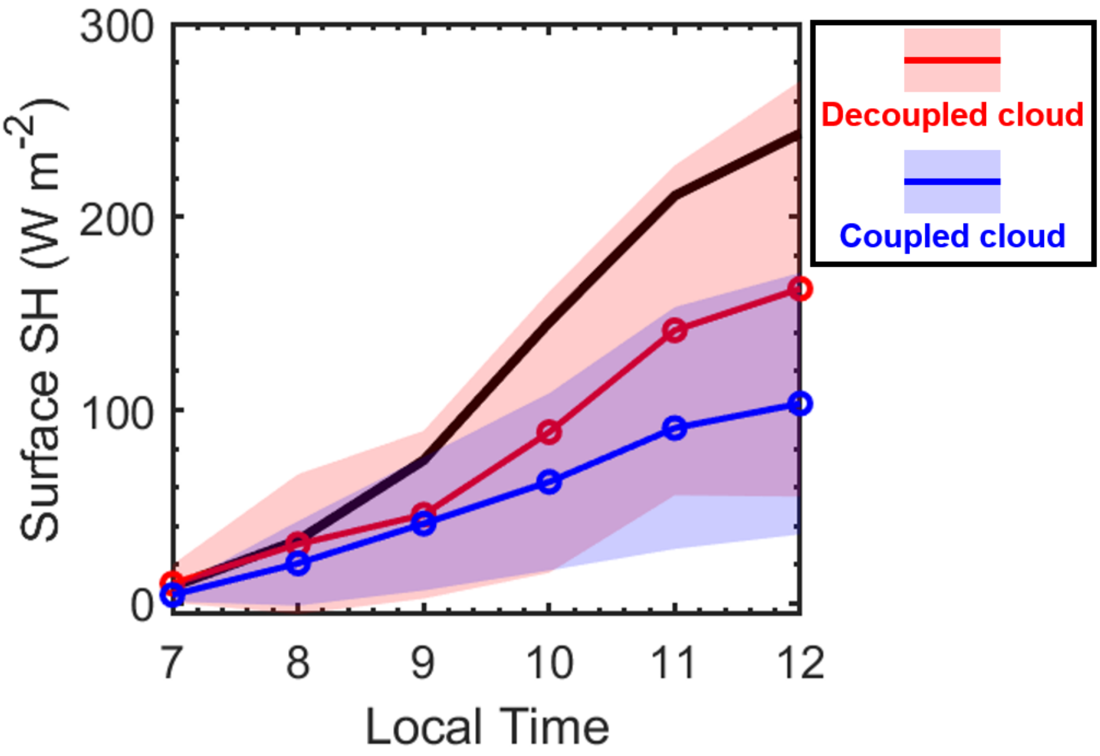

Figure S4. (a) Variations of the surface sensible heat (SH) under coupling (blue) and decoupling (red) conditions during 07:00-12:00 LT. The shaded areas indicate the corresponding standard deviations. Black line indicates the surface SH under the clear-sky condition.

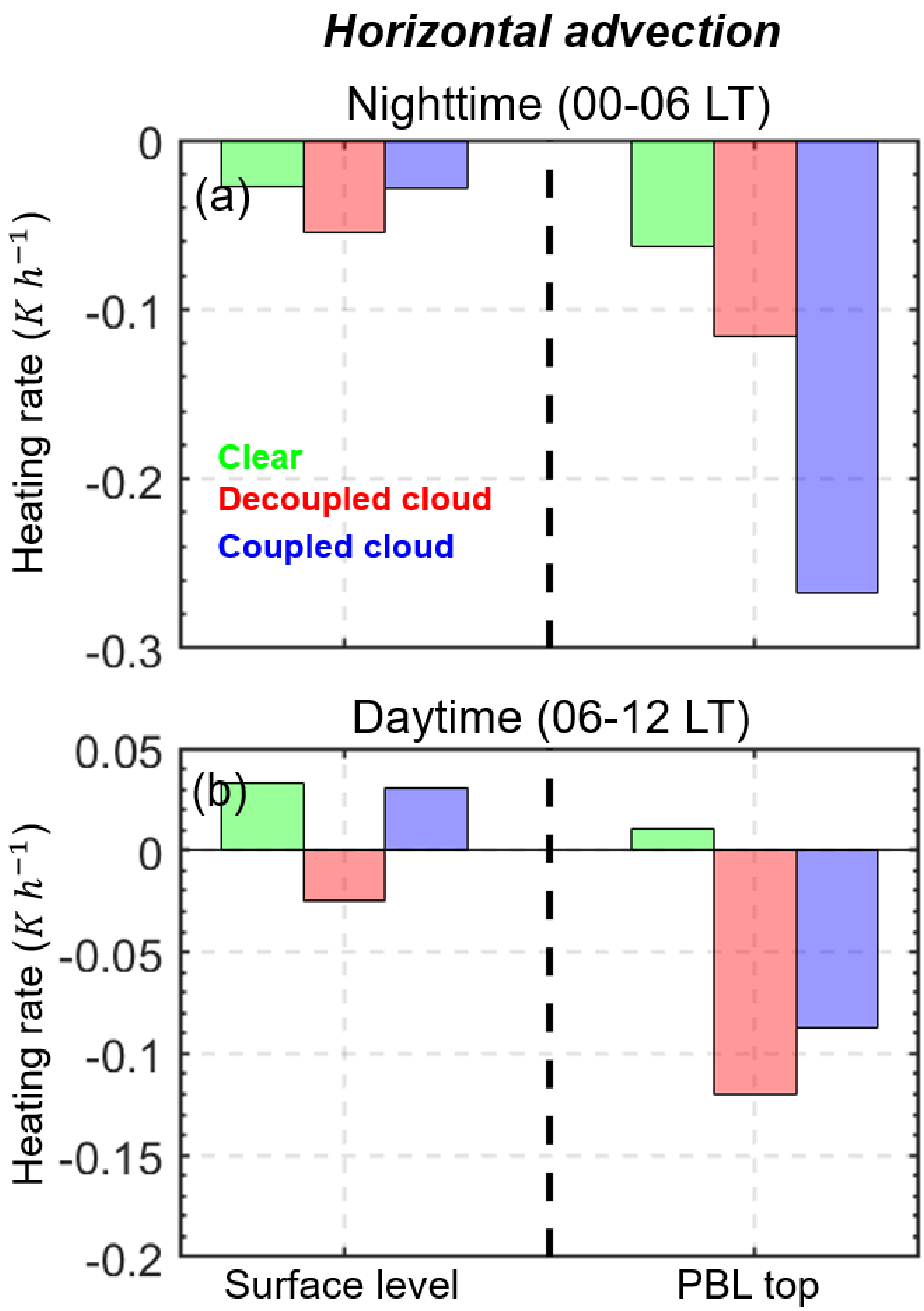

Figure S5. The heating rate due to the horizontal advection at the surface level and the PBL top under the clear sky (green), decoupled cloud conditions (red), and coupled cloud conditions (blue) during (a) the nighttime (00:00-06:00 LT) and (b) the daytime (06:00-12:00 LT). The heating rate due to the horizontal advection is obtained is obtained from National Centers for Environmental Prediction (NCEP) reanalysis data.

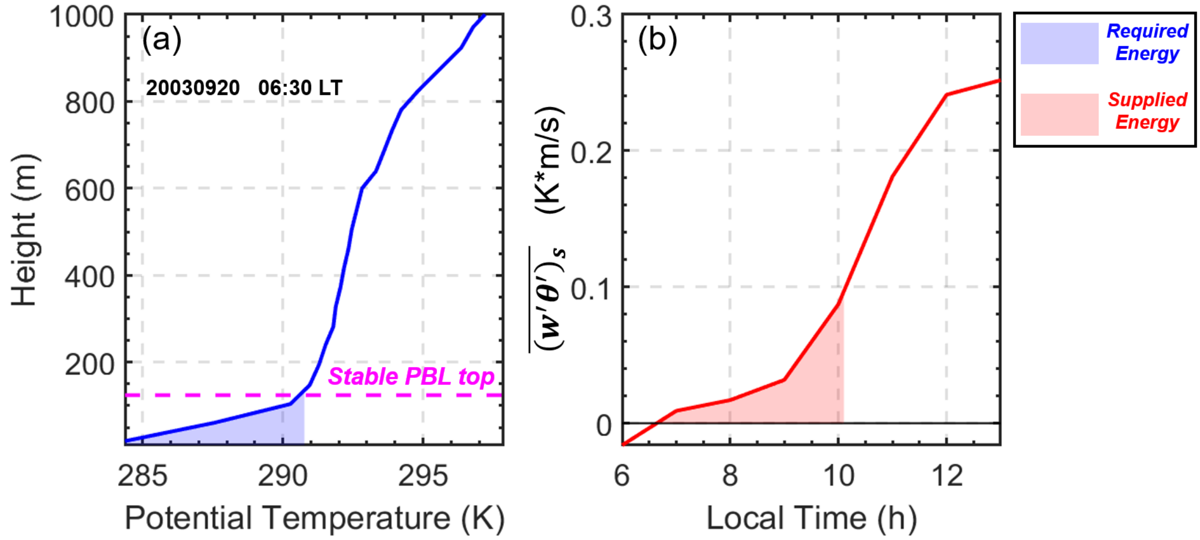

Figure S6. Graphical approach to estimate the required energy and supplied energy for the phase transition. (a) The potential temperature profiles in the early morning. The top of stable PBL is marked as the pink line. (b) The evolution of surface sensible heat during 06:00-13:00 LT. The surface sensible heat flux ($\overline{(w'\theta')_s}$) drives the phase transition, for it supplies the energy to erode the near-surface inversion of potential temperature. Since there is no cloud condensation within PBL, latent heat does not contribute to the PBL phase transition under clear-sky and decoupled conditions. For the phase transition, the supplied energy reaches the required energy as follows: $\rho C_p \int_0^t \overline{(w'\theta')_s}\, dt = \rho C_p \int_{\theta_0}^{\theta_1} z(\theta)\, d\theta$. The magnitude of left side of equation is marked as the blue area in (a), and the magnitude of right side of equation is marked as the red area in (b). For this case, the supplied energy from sensible heat reaches the required energy in 10:03 LT, leading the phase transition of PBL. This method focuses the effects of surface forcing but neglect the contributions of advection. From statistical point of view, the contribution of horizontal advection is an order of magnitude smaller than the contribution of surface heating (Figure S5, Figure 3).

References

Clothiaux, E. E., Ackerman, T. P., Mace, G. G., Moran, K. P., Marchand, R. T., Miller, M. A., & Martner, B. E. (2000). Objective determination of cloud heights and radar reflectivities using a combination of active remote sensors at the ARM CART sites. Journal of Applied Meteorology, 39(5), 645-665.

Flynn, D., Shi, Y., Lim, K., & Riihimaki, L. (2017). Cloud Type Classification (cldtype) Value-Added Product. Ed. by Robert Stafford, ARM Research Facility. DOE/SC-ARM-TR-200.

Holdridge, D., Ritsche, M., Prell, J., and Coulter, R. (2011): Balloon-borne sounding system (SONDE) handbook, https://www.arm.gov/capabilities/instruments/sonde.

Kollias, P., Clothiaux, E. E., Miller, M. A., Albrecht, B. A., Stephens, G. L., & Ackerman, T. P. (2007). Millimeter-wavelength radars: New frontier in atmospheric cloud and precipitation research. Bulletin of the American Meteorological Society, 88(10), 1608-1624.

Liu, S., & Liang, X. Z. (2010). Observed diurnal cycle climatology of planetary boundary layer height. Journal of Climate, 23(21), 5790-5809.

Long, C. N., & Shi, Y. (2008). An automated quality assessment and control algorithm for surface radiation measurements. The Open Atmospheric Science Journal, 2(1).

Rodriguez, J.D., Perez, A. and Lozano, J.A. (2009). Sensitivity analysis of k-fold cross validation in prediction error estimation. IEEE transactions on pattern analysis and machine intelligence, 32(3), pp.569-575.

Tang, S., Xie, S., Zhang, M., Tang, Q., Zhang, Y., Klein, S. A., ... & Sullivan, R. C. (2019). Differences in eddy-correlation and energy-balance surface turbulent heat flux measurements and their impacts on the large-scale forcing fields at the ARM SGP site. Journal of Geophysical Research: Atmospheres, 124(6), 3301-3318.

Wesely, M. L., Cook, D. R., and Coulter, R. L. (1995): Surface heat flux data from energy balance Bowen ratio systems (No. ANL/ER/CP-84065; CONF-9503104-2). Argonne National Lab., IL (United States).

Zheng, Y., Rosenfeld, D., & Li, Z. (2018). The relationships between cloud top radiative cooling rates, surface latent heat fluxes, and cloud-base heights in marine stratocumulus. Journal of Geophysical Research: Atmospheres, 123(20), 11-678.